The forward rainbow scattering of low energy protons by a graphene sheet

M. Ćosić[1], M. Hadžijojić[1], R. Rymzhanov[2], S. Petrović[1], and S. Bellucci[3]

[1]Vinča Institute of Nuclear Sciences, University of Belgrade, P. O. Box 522, 11001 Belgrade, Serbia
[2]Joint Institute for Nuclear Research, Joliot-Curie st. 6, 141980 Dubna, Moscow Region, Russia,
[3] Laboratori Nazionali di Frascati LNF, INFN - Istituto Nazionale di Fisica Nucleare, Via Enrico Fermi 40 - 00044 Frascati (Roma) Italy

Nanoscience and Nanotechnology 2018.

Table of content

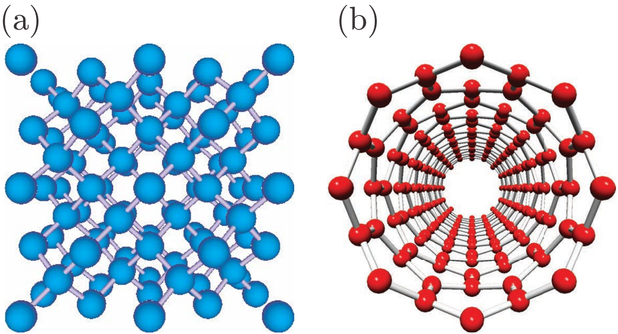

Figure 1: The view of: (a) the Si crystal in direction of the $[1, 0, 0]$ axis. (b) The view of the zig-zag single wall carbon nanotube (SWCNT) in direction of the SWCNT axis.

Ion Channeling Effect

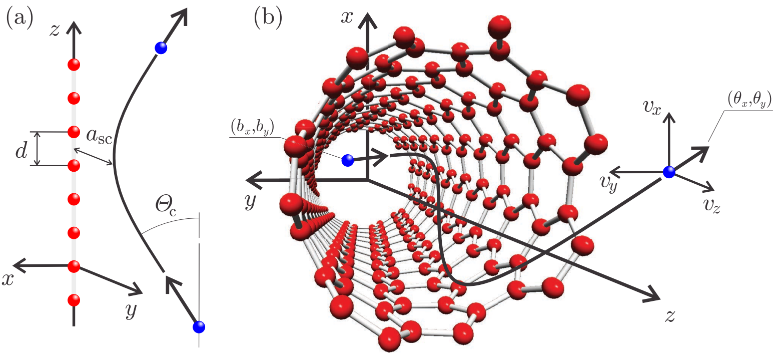

Figure 2: (a) Ion scattering by atomic string. (b) Schematic of the ion channeling process.

Potential of ion-solid interaction V is build up from ion atom potential φ:

$$V(\boldsymbol{r}) \approx \sum_s \frac{1}{d} \int_z \varphi(\boldsymbol{r} - \boldsymbol{\rho}_s) dz.$$

The Prototype of the Rainbow Effect

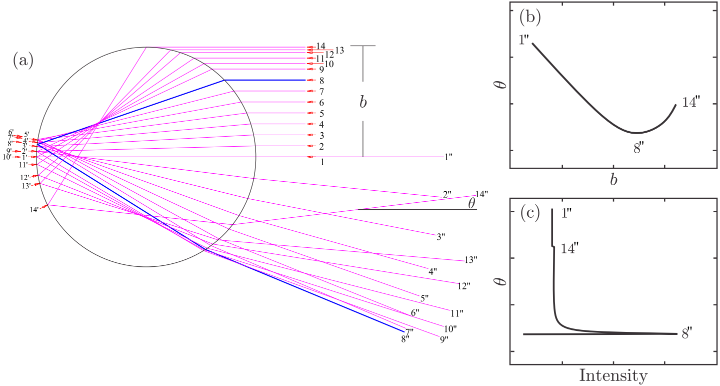

Figure 3: (a) Light rays in a droplet of water, the blue ray is the rainbow ray. (b) The deflection function $\theta(b)$. (c) Intensity of light.

Differential cross-section of scattering process is

$$\sigma_{\text{diff}}^{\theta} \sim \left(\frac{d\theta}{db}\right)^{-1}\Bigg|_{b_8} \to \infty.$$

Theory of Rainbow Scattering

Solution of equation of motion

$$m\frac{d^2\boldsymbol{r}}{dt^2} = -\nabla U(\boldsymbol{r}),$$

where U is thermally averaged potential

$$U(\boldsymbol{r}) = \frac{1}{(2\pi\|\boldsymbol{\Sigma}\|)^{3/2}} \int_{\boldsymbol{r}'} V(\boldsymbol{r}-\boldsymbol{r}') \exp\left(-\frac{1}{2}\boldsymbol{r}'^{T}\cdot\boldsymbol{\Sigma}^{-1}\cdot\boldsymbol{r}'\right) \mathrm{d}^3\boldsymbol{r}',$$

define mappings

$$\theta_x = \theta_x(\boldsymbol{b}), \quad \theta_y = \theta_y(\boldsymbol{b});$$

where $\theta_x \approx v_x/v_z$ and $\theta_y \approx v_y/v_z$.

$$\sigma^{\theta}_{\mathrm{diff}} = \frac{1}{|J_\theta|}, \quad J_\theta = \frac{\partial\theta_x}{\partial b_x}\frac{\partial\theta_y}{\partial b_y} - \frac{\partial\theta_x}{\partial b_y}\frac{\partial\theta_y}{\partial b_x}.$$

Rainbow lines in IP plane are solutions of equation $J_\theta = 0$. Their image in the final transmitted angle planes are called angular rainbows.

Rainbows in chiral SWCNT

The covariance matrix is modeled according Debye theory,

$$\boldsymbol{\Sigma} = \frac{3\hbar^2}{M_c m_u k_B \Theta_B}\left[\frac{\mathfrak{D}_f(\Theta_D/T)}{\Theta_D/T} + \frac{1}{4}\right]$$

where $\mathfrak{D}_f$ is Debye function.

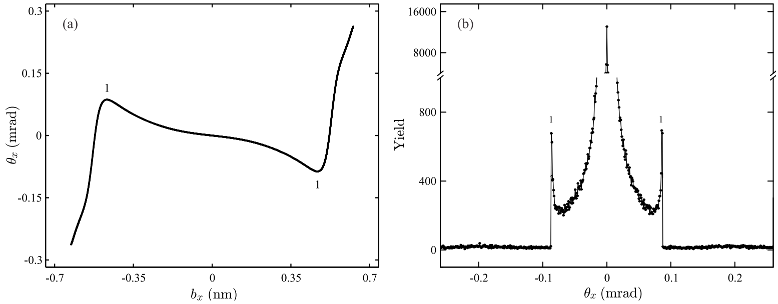

Figure 4: (a) The angular deflection function of 1-GeV protons transmitted through 10-μm long chiral SWCNT $(11, 9)$. (b) The corresponding angular distribution.

Rainbows in thin Si crystal

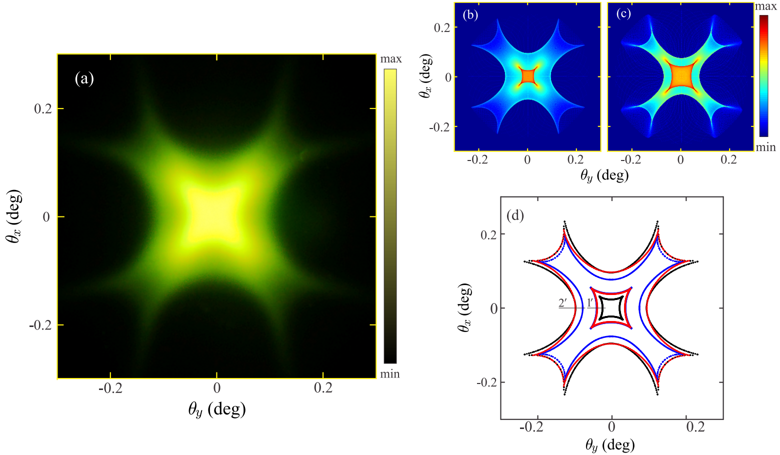

Figure 5: (a) Experimental distribution of 2-MeV protons transmitted through ⟨100⟩ channel of 55-nm thick Si crystal. Theoretical distributions for: (b) ZBL and (c) Molière's potential. (d) Corresponding rainbow lines.

Proton-Graphene interaction

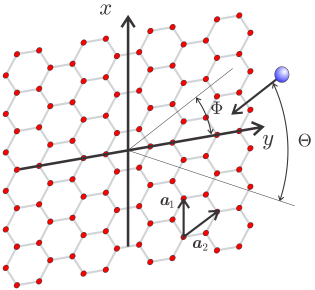

Figure 6: Schematic of the proton transmission through graphene.

- For 5-keV protons de Broglie wavelength is $\lambda = 4.0476 \times 10^{-4}$ nm.
- Interaction potential calculated starting from Doyl-Turner's ZBL and Molière's potential.
- Energy loss is negligible, neutralization probability $\approx 40\%$
- Matrix $\boldsymbol{\Sigma}$ modeled according to Debye theory and calculated using molecular dynamic approach.

Proton-graphene interaction potential

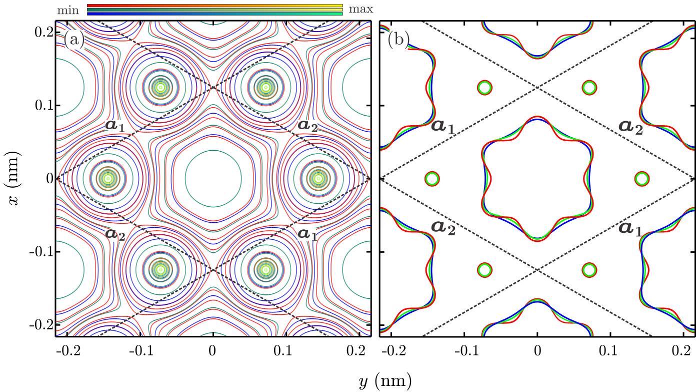

Figure 7: (a) Contour lines of the proton-graphene interaction potential in the plane $z = 0$, for: $U^{DT}(\boldsymbol{r})$, $U^{ZBL}(\boldsymbol{r})$, and (c) $U^{M}(\boldsymbol{r})$ potentials shown by different hues of the red, green and blue color respectively. (b) Corresponding zero-curvature lines shown by red, green, and blue lines respectively. The black dashed rhombus denotes the graphene unit cell.

Proton trajectories

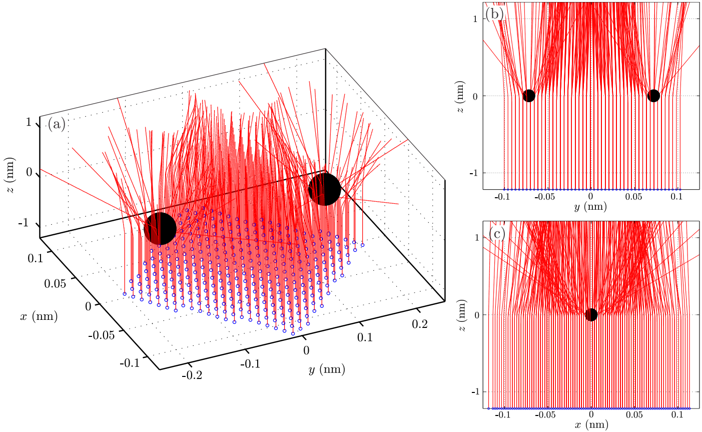

Figure 8: Proton trajectories entering the interaction interval of the graphene unit cell for $U^{DT}(\boldsymbol{r})$ potential. Entrance points are denoted by open small blue circles. Black spheres indicate positions of the carbon atoms.

Ideal rainbow patterns

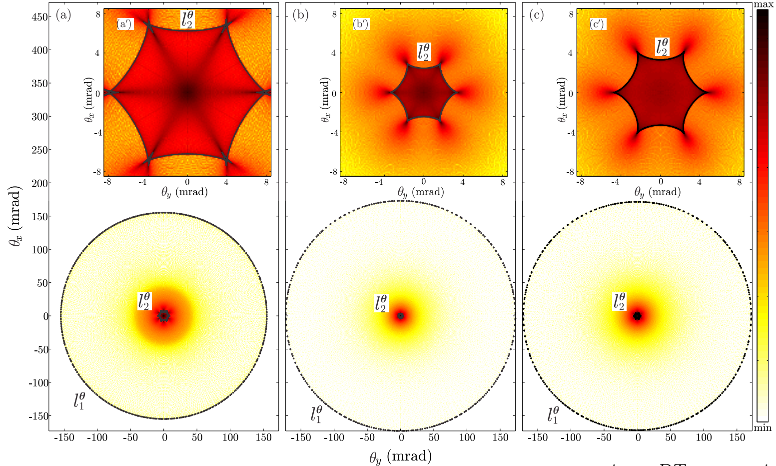

Figure 9: Angular yields of transmitted protons for: (a^i) $U^{DT}(\boldsymbol{r})$; (b^i) $U^{ZBL}(\boldsymbol{r})$; and (c^i), $U^M(\boldsymbol{r})$ potentials, and $\boldsymbol{\Sigma} = 17.37$ pm^2. Rainbow lines are shown by doted black lines. Insets (a^{ii}), (b^{ii}), and (c^{ii}) show enlarged parts of proton yields around the rainbow line l_2^θ.

Real rainbow patterns

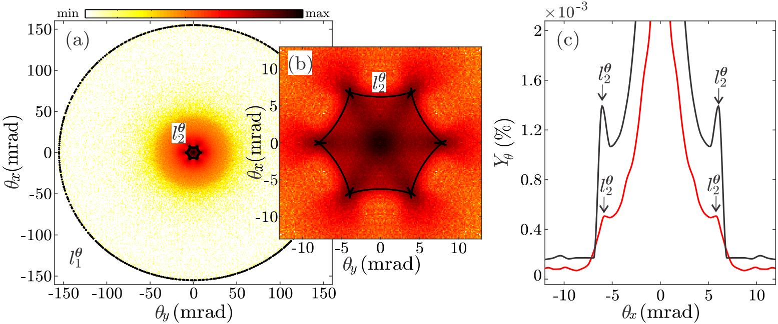

Figure 10: (a) Angular yield of the proton beam having divergence of 1 mrad, and for $U^{DT}(\boldsymbol{r})$ potential. (b) Enlarged part of proton yield around the rainbow line l_2^θ. Rainbow lines are shown by the doted black line. (c) Vertical cross-sections through yields from graph (b), and from the Fig. 9(a) — the red and the black line, respectively.

Calculation of graphene thermal motion

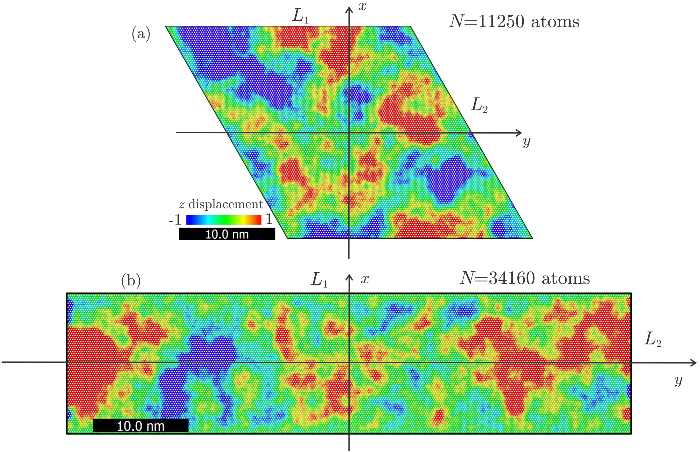

Figure 11: State of the computational supercell for: (a) rhombic cell with periodic boundary conditions representing infinite graphene sheet; and (b) rectangular cell with combination of periodic and fixed boundary conditions representing graphene nanoribon.

The steady state of graphene thermal motion

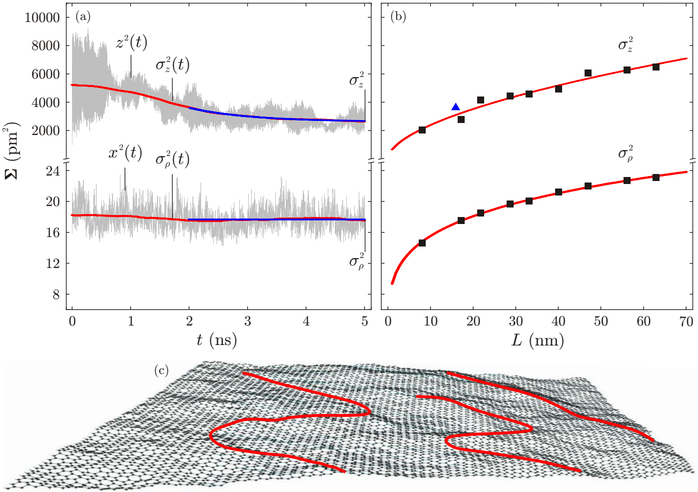

Figure 12: (a) Time dependency of the matrix $\mathbf{\Sigma}(t)$ components. (b) Scaling of $\mathbf{\Sigma}$ with linear super-cell size $L = \sqrt{L_1 L_2}$. (c) State of the graphene sheet at t = 2.9 ns, showing sheet ripples.

Evolution of the rainbow pattern for $\boldsymbol{\Sigma} = \sigma \boldsymbol{I}$

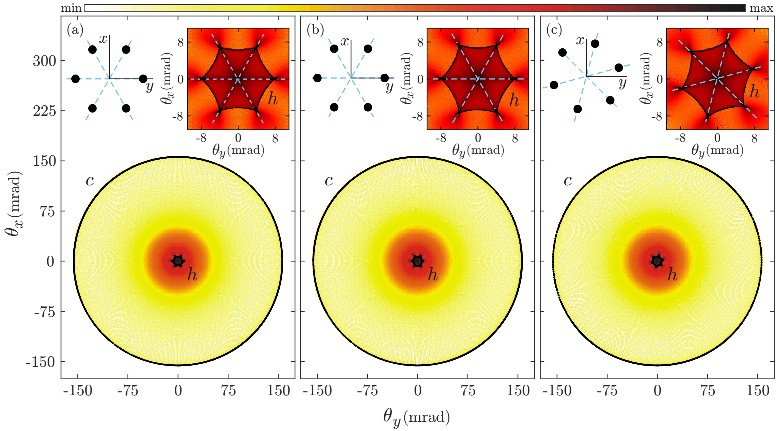

Figure 13: Rainbow patterns and angular yields of transmitted protons for $\boldsymbol{\Sigma} = 17.37$ pm^2 and tilt angles: (a) $(\Theta, \Phi) = (0, 0)$; (b) $(\Theta, \Phi) = (0.065, 0)\pi$ rad; and (c) $(\Theta, \Phi) = (0.065, 0.25)\pi$ rad. Insets show projections of the graphene hexagon to the transverse plane, and enlarged central parts of distributions.

Evolution of rainbow pattern for $\mathbf{\Sigma} = \mathrm{diag}(\sigma_\rho^2, \sigma_\rho^2, \sigma_z^2)$

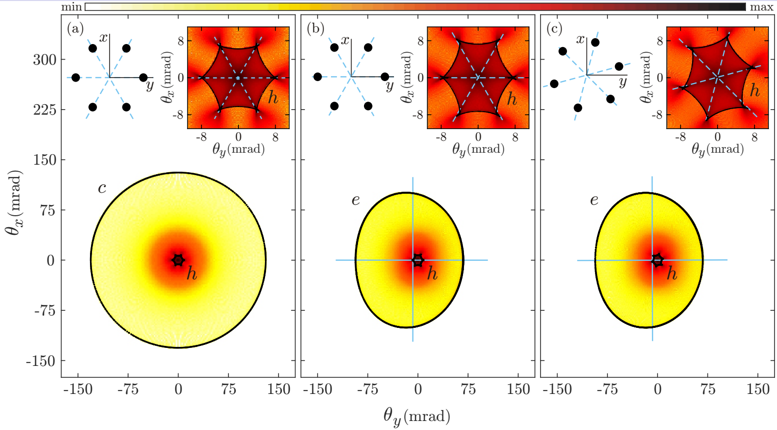

Figure 14: Rainbow patterns and angular yields of transmitted protons for $\mathbf{\Sigma} = \mathrm{diag}(17.67, 17.67, 2619.10)$ pm^2 and tilt angles: (a) $(\Theta, \Phi) = (0, 0)$; (b) $(\Theta, \Phi) = (0.065, 0)\pi$ rad; and (c) $(\Theta, \Phi) = (0.065, 0.25)\pi$ rad. Insets show projections of the graphene hexagon to the transverse plane, and enlarged central parts of distributions.

Evolution of rainbow pattern for $\boldsymbol{\Sigma} = \mathrm{diag}(\sigma_x^2, \sigma_y^2, \sigma_z^2)$

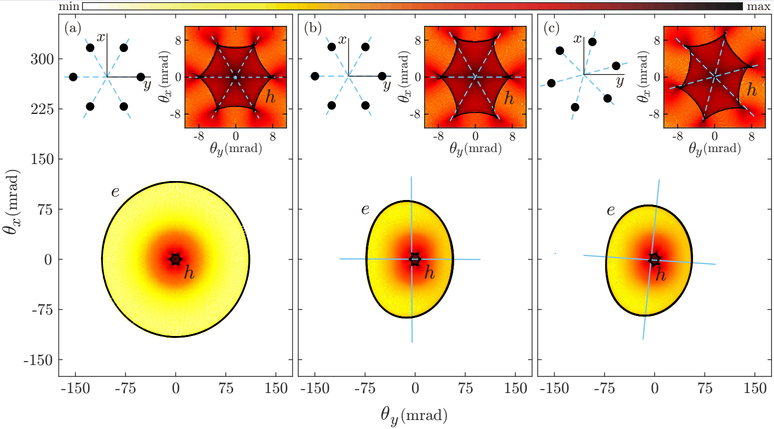

Figure 15: Rainbow patterns and angular yields of transmitted protons for $\boldsymbol{\Sigma} = \mathrm{diag}(18.14, 35.45, 3698.18)$ pm^2 and tilt angles: (a) $(\Theta, \Phi) = (0, 0)$; (b) $(\Theta, \Phi) = (0.065, 0)\pi$ rad, and (c) $(\Theta, \Phi) = (0.065, 0.25)\pi$ rad. Insets show projections of the graphene hexagon to the transverse plane, and enlarged central parts of distributions.

Reconstruction of the covariance matrix

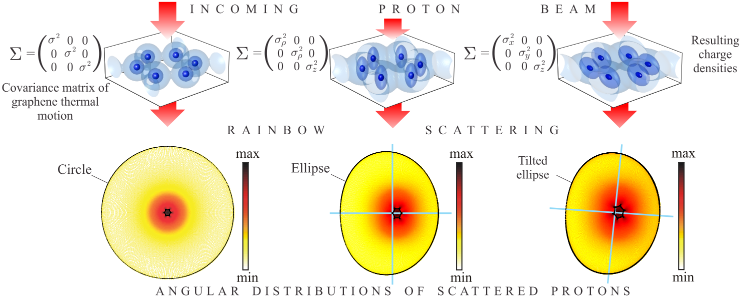

Figure 16: Schematics of the identification of the covariance matrix $\boldsymbol{\Sigma}$ form, which reduces to investigation of the outer rainbow pattern for different sample orientations.

Conclusions

- Rainbow scattering occurs in transmission of the 5-keV protons through graphene.
- Rainbow pattern consists of two parts the outer formed by protons experiencing close collisions with carbon atoms and the inner formed by protons scattered by graphene hexagon.
- Inner pattern is very sensitive to changes in proton-carbon interaction and are practically insensitive to the thermal vibrations.
- Outer rainbow lines are very sensitive to the thermal vibrations.
- Graphene rainbow lines could be used for determination of the proton-carbon interaction potential and for determination of the Debye-Waller form factor.